24th COBEM - 2017

24th ABCM International Congress of Mechanical Engineering
December 3-8, 2017, Curitiba, PR, Brazil

COBEM-2017-2619
COMPRESSIBLE FLOW OVER A CIRCULAR CYLINDER USING A VIRTUAL BOUNDARY METHOD

J. Solarte-Pineda
P.C. Greco-Junior
Departamento de Engenharia Mecânica, USP - 13566-590, São Carlos, SP
jsp@sc.usp.br, pcgreco@usp.br

Abstract. *The aim of this work is to present a fluid-structure interaction method, known as virtual boundary method developed for flow modeling. The main purpose is to analyze the behavior of inviscid, compressible flow over a circular cylinder. The virtual boundary method uses two independent grids, one for the fluid and one for the embedded body, where the boundary condition at the surface of the body, is imposed at each time step using calculated body force components of the momentum equations. The solution, is given by a second order of precision, in both space and time, predictor-corrector scheme. The method has several advantages when compared with other CFD methods. The grid generation algorithms for both grids are easy to write and implement, with low computational cost, and complex geometries can be easily modeled. The results are presented in subsonic, transonic and supersonic conditions, showing that, even though the model is inviscid, some characteristics of viscous flow appear in the result due to implicit and artificial viscosity, added to avoid stability problems.*

Keywords: *CFD, Virtual boundary, Body force, Circular cylinder, Compressible flow.*

1. INTRODUCTION

The fluid-structure interaction methods has increased in popularity in the last decades, due the improvement in grid generation for complex geometries in the field of CFD *(Computational Fluid Dynamics).* Peskin (1972) is known for the first work using the immersed boundary method *(IBM).* In Peskin (1977), the method was used to analyze the behavior of the blood within the human heart, where the blood was modeled as a non newtonian fluid, and the heart as a viscoelastic membrane, at low Reynolds numbers. Peskin (2003) describes the IBM as a fluid-structure interaction method, with a new mathematical approach and numerical scheme. The main characteristics of the IBM compared with common CFD approaches are that two grids are used instead of just one geometry conforming one, and that the boundary condition on the surface of the embedded body is not directly imposed. Rather, there is a function which computes a body force needed to generate the no slip boundary condition. A usual function used by Goldstein *et al.* (1993) and Saiki and Biringen (1996) is given by

$$f(x_s,t) = \alpha \int_0^t [u(x_s,t) - V(x_s,t)]dt + \beta[u(x_s,t) - V(x_s,t)]. \tag{1}$$

In Eq. 1 $f(x_s,t)$ is the body force necessary for the no slip boundary condition. x_s are coordinates of the embedded body, α and β are negative constants representing a system with spring and damper. $V(x_s,t)$ is the velocity at the surface of the embedded body. However, there is a problem with the use of Eq. 1. The values for constants α and β are arbitrarily chosen and, in some cases, divergence may occur. One alternative solution for imposing the boundary condition was given by Mohd-yusof (1997) in which the body force is directly computed at each time step from the momentum equation.

In the classical immersed boundary method the body may move or deform. Goldstein et al. use the same approach as the IBM with the difference that the body has fixed boundaries, known as virtual boundary method *(VBM).* The main advantage, of the IBM is that the grid generation algorithms are easy to write and implement when compared with conforming grid algorithms. Due to the versatility of this method several authors have been working with it. Since the two grids are independent, it is easy to work with complex geometries. Indeed, with this approach, it is very simple to model rigid and flexible bodies. Several works in the literature prove this statement right. As examples (Fadlun *et al.*, 2000) analyzes the flow inside a piston engine combustion chamber, (Choi *et al.*, 2007) analyzes the vortex generation in air due the human body motion, (Ghias *et al.*, 2007) analyzes the wing tip vortex for a rectangular wing. Despite the advantages, the IBM methods can present some problems with the smoothness for the results in the region close to the interface between the fluid and the body. That happens because, for complex geometries, the grid points of the two grids are usually not coincident, and the precision is normally limited to second order on the interface. (Griffith and Peskin,

2005) presents an study of the order of accuracy of the Immersed Boundary Method and (Bonfigli, 2011) was able to reach fourth order of precision in his work.

There are few works using IBM or VBM for compressible flow. As examples we have De Palma *et al.* (2006) using the VBM and solving the Navier-Stokes equations with RANS approximation *(Reynolds Averaged Navier-Stokes)* to analyze the viscous compressible flow over a circular cylinder and a NACA 0012 airfoil in supersonic condition. De Tullio *et al.* (2007), also analyzes the viscous compressible flow over a circular cylinder and a NACA 0012 airfoil in supersonic flow using local mesh refinement near the boundary of the embedded body thus getting better results on the fluid-structure interface. Karimian and Ardakani (2011) uses the finite volume method along with ghost cells inside the body to analyze the compressible inviscid flow over airfoils.

2. NUMERICAL METHODOLOGY

2.1 Governing equations

The mathematical model for an inviscid, adiabatic and compressible flow is represented by the Euler equations which, for two dimensional flow in conservative form, are given by

$$\frac{\partial U}{\partial t} + \frac{\partial F}{\partial x} + \frac{\partial G}{\partial y} = J, \tag{2}$$

where $\frac{\partial}{\partial t}$, $\frac{\partial}{\partial x}$, $\frac{\partial}{\partial y}$ are partial derivatives in space and time respectively, U is the solution vector, F and G are flux vectors, and J is the source vector, given by

$$U = \left[\rho, \rho u, \rho v, \rho\left(e + \frac{\vec{V}^2}{2}\right)\right]^T, \tag{3}$$

$$F = \left[\rho u, \rho u^2 + p, \rho uv, \rho\left(e + \frac{\vec{V}^2}{2}\right)u + pu\right]^T, \tag{4}$$

$$G = \left[\rho v, \rho uv, \rho v^2 + p, \rho\left(e + \frac{\vec{V}^2}{2}\right)v + pv\right]^T, \tag{5}$$

$$J = \left[0, \rho f_x, \rho f_y, \rho\left(uf_x + vf_y\right)\right]^T. \tag{6}$$

$\vec{V}$ is the velocity vector with components u and v, ρ is the density, p is the pressure, and e is the specific internal energy of the fluid. f_x and f_x are body forces. In order to close and solve the system, we need to use some additional equations. The equation of state for an ideal gas given by

$$P = (\gamma - 1)\rho e, \tag{7}$$

is used, where γ is the specific heat ratio. Also for a calorically perfect gas, the relationship between the internal energy and the temperature of the gas is defined by

$$e = C_v T, \tag{8}$$

and C_v is the specific heat at constant volume of the fluid.

2.2 Numerical Approach

Consider a two dimensional flow in a large domain on a Cartesian plane. The governing equation are solved numerically at discrete points in the domain. A simple corrector-predictor method (McCormack) is used. The solution vector U at the time step $n+1$ is given by.

$$U_{i,j}^{n+1} = U_{i,j}^{n} + \left(\frac{\partial U}{\partial t}\right)_{av} \triangle t, \tag{9}$$

where $\left(\frac{\partial U}{\partial t}\right)_{av}$ is the average time derivative of the solution vector U.

$$\left(\frac{\partial U}{\partial t}\right)_{av} = \frac{1}{2}\left(\left(\frac{\partial U}{\partial t}\right)_{i,j}^{n} + \left(\frac{\bar{\partial U}}{\partial t}\right)_{i,j}^{n+1}\right), \tag{10}$$

2.2.1 Predictor step

In the predictor step, the time derivative of the solution vector is computed using a forward finite difference approach of the flux vectors and the source vector

$$\left(\frac{\partial U}{\partial t}\right)_{i,j}^{n} = J_{i,j}^{n} - \frac{F_{i+1,j}^{n} - F_{i,j}^{n}}{\Delta x} - \frac{G_{i,j+1}^{n} - G_{i,j}^{n}}{\Delta y}, \tag{11}$$

2.2.2 Corrector step

The corrector step, is computed similarly to the predictor step but using a backward finite difference approach, instead forward, and the flux vectors and the source vector are those obtained in the predictor step and denoted by $\bar{F}$ and $\bar{G}$:

$$\left(\frac{\partial \bar{U}}{\partial t}\right)_{i,j}^{n+1} = J_{i,j}^{n} - \frac{\bar{F}_{i,j}^{n+1} - \bar{F}_{i-1,j}^{n+1}}{\Delta x} - \frac{\bar{G}_{i,j}^{n+1} - \bar{G}_{i,j-1}^{n+1}}{\Delta y}, \tag{12}$$

2.3 Body Force

Mohd-yusof (1997) describes a direct forcing method to solve the compressible Navier-Stokes equations. Using the time discrete momentum equation in the explicit form

$$\frac{u^{n+1} - u^{n}}{\Delta t} = RHS^{n} + f^{n+1}, \tag{13}$$

where RHS has the pressure gradient and the advection and viscous terms. The body force necessary to impose the velocity boundary condition at the surface of the embedded body for the Navier-Stokes equations $(u = 0, v = 0, w = 0)$ is calculated by adjusting the velocity u^{n+1}. Then the body force f^{n+1} is calculated from Eq. 13.

$$f^{n+1} = \frac{u^{n+1} - u^{n}}{\Delta t} - RHS^{n}. \tag{14}$$

In the present study, the same principle is used with modifications so to work with inviscid compressible flow. Again the momentum equations are used to calculate the body force. Equations 15 and 16 are the momentum equations in x and y directions:

$$\frac{\partial(\rho u)}{\partial t} + \nabla \cdot (\rho u \vec{V}) = -\frac{\partial p}{\partial x} + \rho f_x, \tag{15}$$

$$\frac{\partial(\rho v)}{\partial t} + \nabla \cdot (\rho v \vec{V}) = -\frac{\partial p}{\partial y} + \rho f_y, \tag{16}$$

The body forces, in the x and y directions, are calculated by solving Eqs. 15 and 16 for fx and fy.

$$f_x = \frac{\rho\frac{\partial u}{\partial t} + u\frac{\partial \rho}{\partial t} + 2\rho u\frac{\partial u}{\partial x} + u^2\frac{\partial \rho}{\partial x} + \rho v\frac{\partial u}{\partial y} + \rho u\frac{\partial v}{\partial y} + uv\frac{\partial \rho}{\partial y} + \frac{\partial p}{\partial x}}{\rho}, \tag{17}$$

$$f_y = \frac{\rho\frac{\partial v}{\partial t} + v\frac{\partial \rho}{\partial t} + 2\rho v\frac{\partial v}{\partial y} + v^2\frac{\partial \rho}{\partial y} + \rho u\frac{\partial v}{\partial x} + \rho v\frac{\partial u}{\partial x} + uv\frac{\partial \rho}{\partial x} + \frac{\partial p}{\partial y}}{\rho}. \tag{18}$$

Finally, the time derivatives of the velocity vector u and v are replaced by.

$$\frac{\partial u}{\partial t} = \frac{u^{n+1} - u^{n}}{\triangle t}, \tag{19}$$

$$\frac{\partial v}{\partial t} = \frac{v^{n+1} - v^{n}}{\triangle t}. \tag{20}$$

2.4 Data Exchange Between the Grids

With the predictor-corrector method the properties of the flow, velocity, density and internal energy, are calculated on the eulerian grid. The fluid properties are needed on the lagrangian grid to allow calculation of the tangential velocity component at the surface and to impose the boundary condition. That process is carried out as follows:

1. Given the lagrangian grid points with equidistant spacing Δs, the eulerian grid is generated over the lagrangian grid with the same spacing as the lagrangian points in both x and y directions ($\Delta s = \Delta x = \Delta y$).
2. For each lagrangian point, three points are created in a normal direction of the surface of the embedded body, with spacing Δx between them (Figure 1(a)).
3. The four closest neighbor points are identified for each normal point, on the eulerian grid (Figure 1(b)).
4. With the four neighbours, the velocity components on the eulerian grid are interpolated to the normal points with a straightforward bilinear interpolation process.
5. With the velocity components at each normal point, the value of the velocity components at the surface of the embedded body (lagrangian grid) are approximated using a Taylor series.

$$u_{(i+1)} = u_i + \frac{\partial u}{\partial n}\Delta n + \frac{\partial^2 u}{\partial n^2}\frac{\Delta n^2}{2!}, \tag{21}$$

$$v_{(i+1)} = v_i + \frac{\partial v}{\partial n}\Delta n + \frac{\partial^2 v}{\partial n^2}\frac{\Delta n^2}{2!}. \tag{22}$$

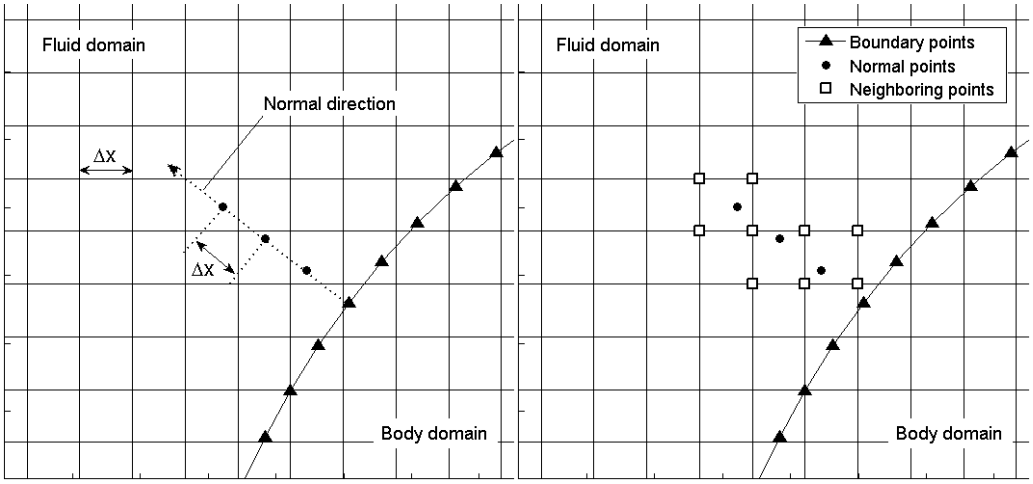

Figure 1: Schematic representation of the data exchange between the grids

3. RESULTS

3.1 Setup

The domain properties are set according to the International Standard Atmosphere. To reduce the total number of grid points of the eulerian mesh, thus reducing the simulation time, a stretching mesh was used, with stretch factor of 1.04. Figure 2(a) shows both the lagrangian and eulerian meshes. Figure 2(b) is a closer view of the circular cylinder. Fig 2(a) and Fig 2(b) are plotted showing only one in four grid points to improve visualization.

3.2 Incompressible Flow

A circular cylinder embedded in a two dimensional, inviscid, incompressible and irrotational flow, can be analyzed by the potential theory of fluid mechanics. Is this case the pressure coefficient varies with the azimuthal angle, θ, through the relationship $cp(\theta) = 1 - 4\sin^2(\theta)$. The VBM, was used to compute the pressure coefficient distribution for a free stream velocity of $V_\infty = 20[m/s]$ with an equivalent Mach number, $M_\infty = 0.06$, low enough to display an incompressible flow behavior for the compressible flow code.
Figure 4.3 shows the distribution of the coefficient of pressure for analytical, experimental and VBM solutions for half of a circular cylinder, the experimental results are taken from Gowen and Perkins (1953). The analytical solution follows the sine function and the flow remains attached to the surface everywhere. There is no wake. The experimental solution for Mach nunber equal to $M_\infty = 0.06$ seem to have a similar behavior that the VMB solutions from 0 to 100 degrees, for both solution the flow In the frontal part of the cylinder remains attached to the surface, with a favorable pressure gradient

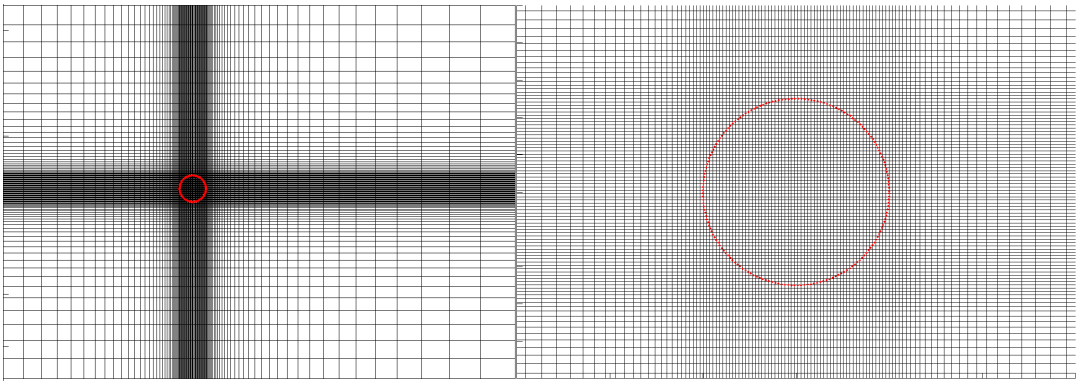

(a) (b)

Figure 2: eulerian and lagrangian grids

while in the rear part for angles between about 142 and 180 degrees and with an adverse pressure gradient, the flow becomes detached from the surface of the cylinder creating a wake, nevertheless the flow detached at different pressure coefficient values for the experimental result the Cp is lower that zero while in the VBM the Cp is greater that zero. in this region the VBM solution lies between the analytical and the experimental solution.

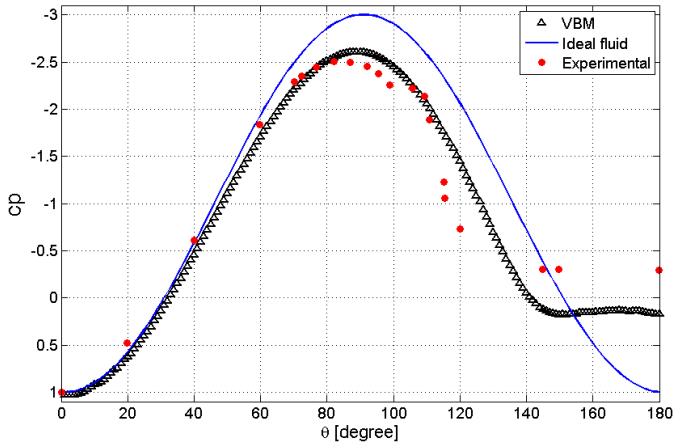

(a)

Figure 3: Pressure coefficients for a incompressible flow

3.3 Compressible flow

3.3.1 Transonic flow

The transonic flow over the circular cylinder using the VBM is presented in this section. The free stream Mach number is $M = 0.5$. For this Mach number the flow accelerates to supersonic velocities at the top and bottom of the cylinder. The flow variables vary periodically, with shock waves oscillating in position and intensity both function of time. behind the shock waves, the flow separates from the surface of the cylinder, at this points the flow reverse the direction of the velocity vector and the flow at the wake becomes highly turbulent. The shock waves induce the flow to detach from the surface. In the rear part of the cylinder the flow is highly rotational. Figure 4 show the Mach number field for several time instants. Where we can see a vortex wake similar to a Von Kármán vortex street showing, again, viscous flow behavior. In Figure 5 show the Mach number at the same instants as the Mach field, after the shock wave the pressure over the separated region is higher than it would be if the flow remained attached. Figure 6 shows the stream lines given by the VBM which are very similar to the results presented by Pandolfi and Larocca (1989). Both solutions are obtained by solving the Euler equations. However, the mathematical approach is different.

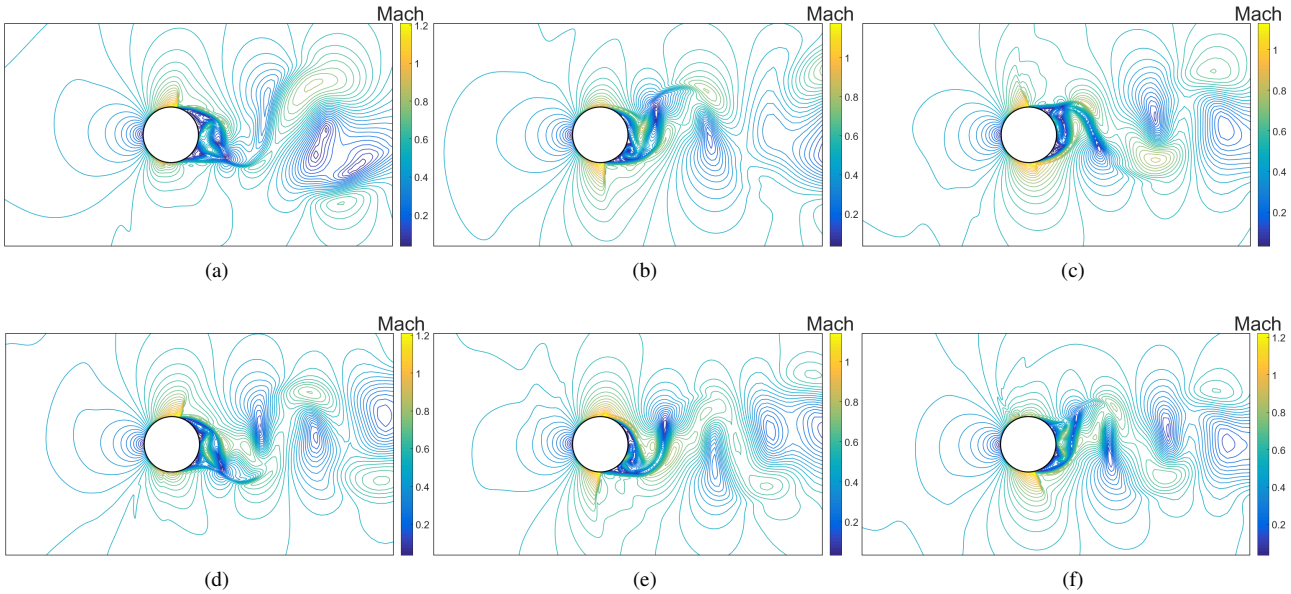

Figure 4: Mach number field, $Mach_\infty = 0.5$ at times (a) 0.5 sg, (b) 0.6 sg, (c) 0.7 sg, (d) 0.8 sg, (e) 0.9 sg, (f) 1.0 sg

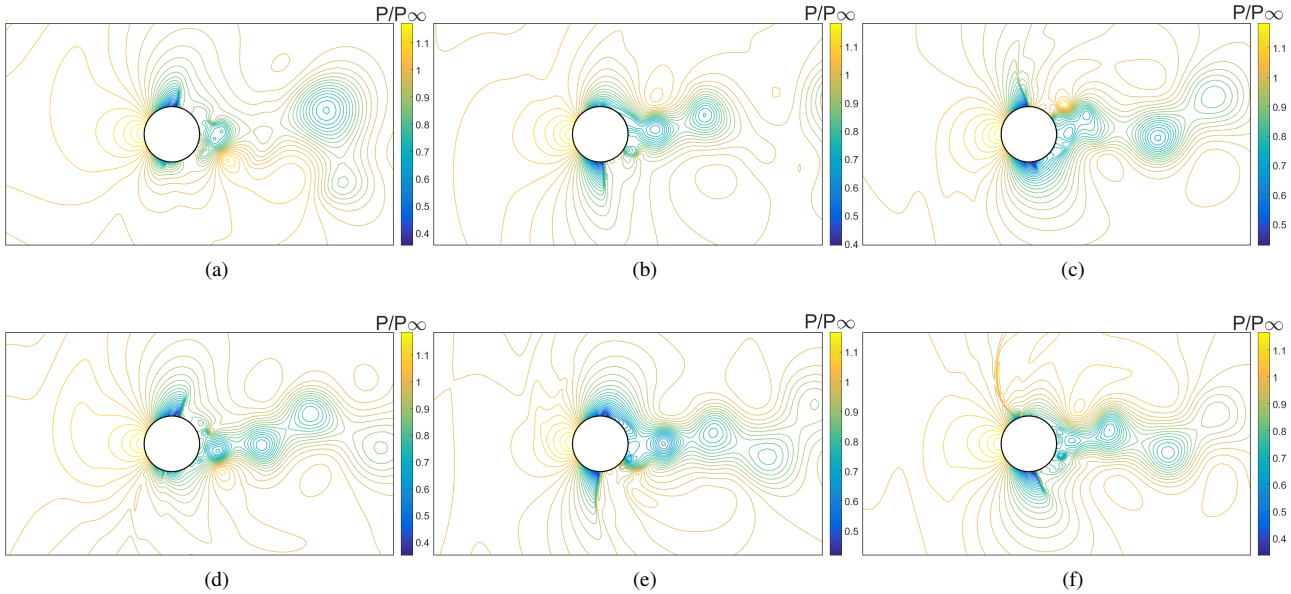

Figure 5: Pressure field, $Mach_\infty = 0.5$ at times (a) 0.5 sg, (b) 0.6 sg, (c) 0.7 sg, (d) 0.8 sg, (e) 0.9 sg, (f) 1.0 sg

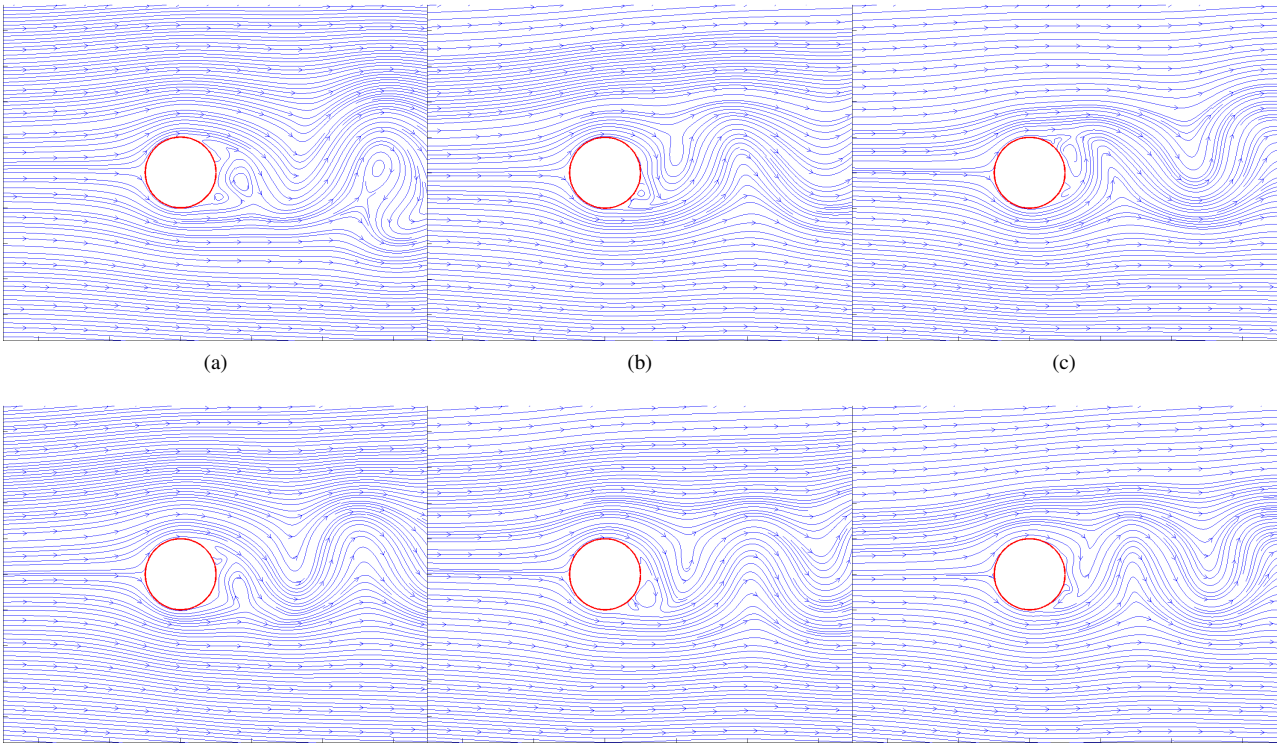

(a) (b) (c)

(d) (e) (f)

Figure 6: Stream lines, $Mach_\infty = 0.5$ at times (a) 0.5 sg, (b) 0.6 sg, (c) 0.7 sg, (d) 0.8 sg, (e) 0.9 sg, (f) 1.0 sg

3.3.2 Supersonic flow

Figure 7.a and 7.b shows the Mach number and pressure field for supersonic flow around a circular cylinder with free stream Mach number $M_\infty = 1.98$, placed in order to compare with experimental results. The classical behavior of blunt bodies is observed, with a detached bow shock wave and a steady wake. Figure 8. Shows the pressure coefficients for both VBM and experimental results, the VBM results seems to have similar bahavior that the experimental results, from 0 to 120 degrees. Nevertheless for the experimental results the flow de attached from the surface at 120 degrees, while in the VBM solution, the pressure arise form 122 to 125 degrees, which it seems to be formed by a little shock wave, then there is a region of separation flow. notice that the pressure at the front of the circular cylinder (0 degrees) for compressible flow is greater that the incompressible flow reaching values greater that 1. Even though the VBM was modelled with an inviscid approximation the results at high Mach numbers are quite good.

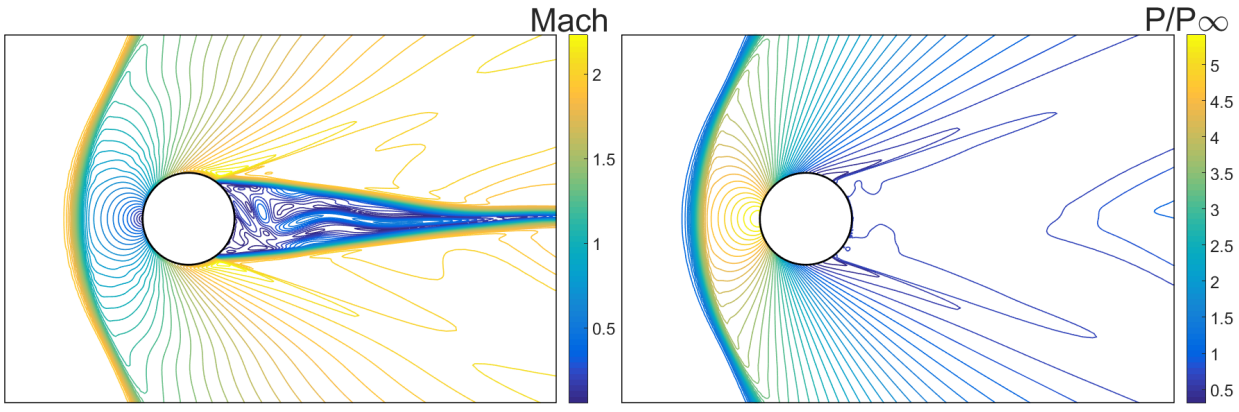

(a) (b)

Figure 7: Supersonic flow over a circular cylinder, $Mach_\infty = 1.98$ (a) Velocity field, (b) Pressure field

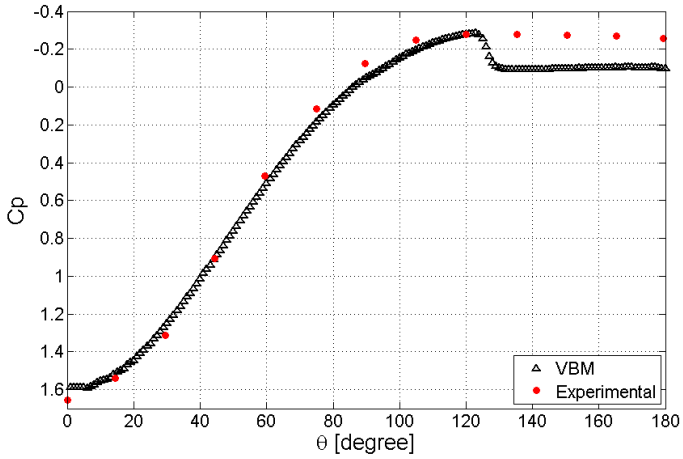

(a)

Figure 8: pressure coefficients VBM and Experimental results Gowen and Perkins (1953)

4. CONCLUSION

The virtual boundary method applied in this work has the advantages of the methods of fluid/structure interaction based on Peskin's method. Relatively complex geometries are easily analyzed in steady and transient conditions as well as moving or static boundaries, even though this study presented results only for static boundaries. However, the same disadvantages encountered by other researchers were found, such as the difficulty to obtain smooth solutions at the interface between the embedded body and the fluid. The inviscid model code, provides an acceptable behavior for all regimens, specially at high Mach numbers where the capture of the shock wave is well defined in both transonic and supersonic conditions. Physical phenomena such as flow separation regions and highly turbulent flow are present. In general, it was seen that new methods like the IBM or the VBM can improve several tasks, like grid generation, becoming part of the CFD field and, applied correctly, can reduce the overall computational cost.

5. REFERENCES

Bonfigli, G., 2011. "High-order finite-difference implementation of the immersed-boundary technique for incompressible flows". *Computers & Fluids*, Vol. 46, No. 1, pp. 2–11.

Choi, J.I., Oberoi, R.C., Edwards, J.R. and Rosati, J.a., 2007. "An immersed boundary method for complex incompressible flows". *Journal of Computational Physics*, Vol. 224, No. 2, pp. 757–784.

De Palma, P., De Tullio, M., Pascazio, G. and Napolitano, M., 2006. "An immersed-boundary method for compressible viscous flows". *Computers & Fluids*, Vol. 35, No. 7, pp. 693–702.

De Tullio, M., De Palma, P., Iaccarino, G., Pascazio, G. and Napolitano, M., 2007. "An immersed boundary method for compressible flows using local grid refinement". *Journal of Computational Physics*, Vol. 225, No. 2, pp. 2098–2117.

Fadlun, E., Verzicco, R., Orlandi, P. and Mohd-Yusof, J., 2000. "Combined Immersed-Boundary Finite-Difference Methods for Three-Dimensional Complex Flow Simulations". *Journal of Computational Physics*, Vol. 161, No. 1, pp. 35–60.

Ghias, R., Mittal, R. and Dong, H., 2007. "A sharp interface immersed boundary method for compressible viscous flows". *Journal of Computational Physics*, Vol. 225, No. 1, pp. 528–553.

Goldstein, D., handler, R. and Sirovich, L., 1993. "modelling a no slip flow boundary with an external force field". *Journal of Computational Physics*, Vol. 105, No. 2, pp. 354–366.

Gowen, F.E. and Perkins, E.W., 1953. *Drag of circular cylinders for a wide range of Reynolds numbers and Mach numbers*. National Advisory Committee for Aeronautics.

Griffith, B.E. and Peskin, C.S., 2005. "On the order of accuracy of the immersed boundary method: Higher order convergence rates for sufficiently smooth problems". *J. Comput. Phys.*, Vol. 208, No. 1, pp. 75–105. ISSN 0021-9991.

Karimian, S.M.H. and Ardakani, M., 2011. "Immersed Boundary Method for the Solution of 2D Inviscid Compressible Flow Using Finite Volume Approach on Moving Cartesian Grid". *Journal of Applied Fluid Mechanics*, Vol. 4, No. 2, pp. 27–36.

Mohd-yusof, 1997. "Combined immersed-boundary / B-spline methods for simulations of ow in complex geometries". *Center for Turbulence Research Annual Research Briefs*, pp. 317–327.

Pandolfi, M. and Larocca, F., 1989. "Transonic flow about a circular cylinder". *Computers & Fluids*, Vol. 17, No. 1, pp. 205 – 220.

Peskin, C.S., 1972. "Flow Patterns Around Heart Valves: A Numerical Method". *Journal of Computational Physics*, Vol. 10, No. 2, pp. 255–271.

Peskin, C.S., 1977. "Numerical analysis of blood flow in the heart". *Journal of Computational Physics*, Vol. 25, No. 3, pp. 220–252.

Peskin, C.S., 2003. "The immersed boundary method". *Acta Numerica*, Vol. 11, pp. 479–517.

Saiki, E. and Biringen, S., 1996. "Numerical simulation of a cylinder in uniform flow: Application of a virtual boundary method". *Journal of Computational Physics*, Vol. 123, No. 2, pp. 450 – 465.

6. RESPONSIBILITY NOTICE

The authors are the only responsible for the printed material included in this paper.